1316 *Inorg. Chem.* **2010**, *49*, 1316–1318
DOI: 10.1021/ic902283g

Inorganic Chemistry
Communication

Salt-Templated Mesoporous Solids Comprised of Interlinked Polyoxovanadate Clusters

Wendy L. Queen, Shiou-Jyh Hwu,* and Shane Reighard

Department of Chemistry, Clemson University, Clemson, South Carolina 29634-0973

Received November 17, 2009

The utility of molten salts has been demonstrated in the synthesis of the first family of mesoporous salt-inclusion solids featuring $[V_4O_{16}]$ and $[V_5O_{17}]$ polyoxovanadate (POV) units interlinked by As^{5+} cations. Despite a high-temperature synthesis, these new solids exhibit unusually porous (~2-nm-diameter) vanadium arsenate frameworks. Disordered metal chloride salts reside inside the pores, leading to relatively large voids (up to ~7.2% of the unit cell volume), which were confirmed by surface area (SA) measurements of the as-prepared polycrystalline samples (~90−110 m^2/g). Given the potential utility of porous POV-containing materials, efforts were made to study changes in the SAs (showing ~35−70% increases) upon salt removal and redox chemistry.

In light of the already proven applications of polyoxometalates (POMs), including catalysis, selective sorption, separations, sensing, molecular recognition, environmental decontamination, and nanotechnology,[1] one can imagine that the development of open-framework materials containing these discrete POMs could have immense promise in many materials applications. In fact, much research has been focused on the deliberate design of POM frameworks with functionalities that include, but are not limited to, mesoporosity and catalytic activity, electronic and ionic transport, ferro- or ferrimagnetism, and photoluminescence.[2]

Most porous frameworks are formed under mild hydrothermal conditions at relatively low temperatures (T < 200 °C).[3] This is because of the low thermal stability of the solvents employed and the expected phase condensation at high temperatures. Among the most notable are the aluminosilicates and synthetic zeolites, which often employ organic templates for the creation of large open frameworks.[3a,c]

Recent reports have shown salt-inclusion chemistry to be an alternative method for the creation of new porous materials at high temperatures (>600 °C).[4] The resulting salt-inclusion solids (SISs) have rigid, thermally stable covalent frameworks integrated with ionic lattices. Like the organic cations in their zeolite counterparts, the salt serves as a template[4d−f] and can be removed by washing with water.[4i] Salt-inclusion chemistry has led to the formation of a new class of special framework solids complementary to those prepared under mild hydro/solvothermal conditions.

Here we report the first series of SISs exhibiting a porous framework featuring ~2-nm-sized channels and relatively high measured surface areas (SAs; ~90−110 m^2/g). The report includes the synthesis, structure, and chemical and physical properties of three families of mesoporous SISs: (salt)·$Cs_{6-n}(V_5O_9)(AsO_4)_2$, where salt = Cs/NaCl, CsBr, or CsI (**V_5** hereafter), (salt)·$Cs_{3.01}(V_{4.6}O_{8.6})(AsO_4)_2$ (**$V_{4/5}$**), and (salt)·$Cs_2(V_4O_8)(AsO_4)_2$ and (salt)·$Cs_{2-2x}(V_4M_xO_8)(AsO_4)_2$ (**V_4**), where M = Cu or Ni and salt = Cs/NaCl. The resulting open frameworks are comprised of [POV]−As^{5+}−[POV] linkages, similar to the [POV]−P^{5+}−[POV] connectivity observed in the previously reported $Cs_3[V_5O_9(PO_4)_2]\cdot xH_2O$ phase. The latter, an isostructural analogue with respect to the covalent lattice, was synthesized under hydrothermal conditions using 1,3-propanediamine as a template.[5]

*To whom correspondence should be addressed. E-mail: shwu@clemson.edu.

(1) (a) Troupis, A.; Triantis, T.; Hiskia, A.; Papaconstantinou, E. *Eur. J. Inorg. Chem.* **2008**, 5579–5586. (b) Zhang, G.; Keita, B.; Craescu, C. T.; Miron, S.; Oliveira, P.; Nadjo, L. *J. Phys. Chem. B* **2007**, *111*(38), 11253–11259. (c) Hiskia, A.; Troupis, A.; Antonaraki, S.; Gkika, E.; Kormalip, P.; Papaconstantinou, E. *Int. J. Environ. Anal. Chem.* **2006**, *86*(3−4), 233–242. (d) Katsoulis, D. *Chem. Rev.* **1998**, *98*(1), 359–387 and references cited therein.

(2) Pope, M. T.; Müller, A. *Polyoxometalate Chemistry from Topology via Self Assembly to Applications*; Springer-Verlag: Berlin, 2001. Online version available at Kluwer Academic Publishers, New York.

(3) (a) van Santen, R. A. *Nature* **2006**, *444*, 46–47. (b) Yu, J.; Xu, R. *Chem. Soc. Rev.* **2006**, *35*, 593–604 and references cited therein. (c) Patarin, J. *Angew. Chem., Int. Ed.* **2004**, *43*, 3878–3880. (d) Hölderich, W.; Hesse, M.; Näumann, F. *Angew. Chem., Int. Ed. Engl.* **1988**, *27*, 226–246.

(4) (a) Queen, W. L.; West, J. P.; Hwu, S.-J.; Van Derveer, D. G.; Zarzyczny, M. C.; Pavlick, R. A. *Angew. Chem., Int. Ed.* **2008**, *47*, 3791–3794. (b) Wang, L.; Hwu, S.-J. *Chem. Mater.* **2007**, *19*, 6212–6221. (c) Wang, L.; Hung, Y.-C.; Hwu, S.-J.; Koo, H.-J.; Whangbo, M.-H. *Chem. Mater.* **2006**, *18*, 1219–1225. (d) Mo, X.; Ferguson, E.; Hwu, S.-J. *Inorg. Chem.* **2005**, *44*, 3121–3126. (e) Mo, X.; Hwu, S.-J. *Inorg. Chem.* **2003**, *42*, 3978–3980. (f) Huang, Q.; Hwu, S.-J. *Inorg. Chem.* **2003**, *42*, 655–657. (g) Hwu, S.-J.; Ulutagay-Kartin, M.; Clayhold, J. A.; Mackay, R.; Wardojo, T. A.; O'Connor, C. T.; Krawiec, M. *J. Am. Chem. Soc.* **2002**, *124*, 12404–12405. (h) Huang, Q.; Hwu, S.-J.; Mo, X. *Angew. Chem., Int. Ed.* **2001**, *40*, 1690–1693. (i) Huang, Q.; Ulutagay, M.; Michener, P. A.; Hwu, S.-J. *J. Am. Chem. Soc.* **1999**, *121*, 10323–10326.

(5) (a) Haushalter, R. C.; Khan, M. I.; Meyer, L. M.; Zubieta, J. A. Microporous square pyramidal−tetrahedral framework vanadium phosphates and their preparation. U.S. Patent 5,602,266, February 11, **1997**. (b) Khan, M. I.; Meyer, L. M.; Haushalter, R. C.; Schweitzer, A. L.; Zubieta, J. A.; Dye, J. L. *Chem. Mater.* **1996**, *8*, 43–53.

Published on Web 01/12/2010

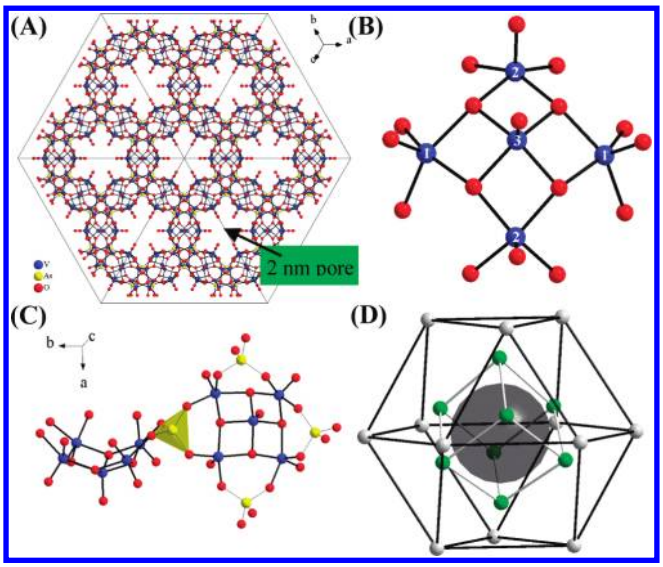

Figure 1. (A) Projected view along [111] of the unit cell showing 2-nm-sized pores. (B) $[V_5O_{17}]$ polyoxovanadate unit. (C) Partial structure of the porous framework made of interconneted $[V_5O_{17}]$ units by As^{5+} cations. (D) $Na@Cl_8@Cs_{12}$ salt unit centered in the pore. Color codes of solid spheres throughout the report: gray, Cs; black, Na; blue, V; yellow, As; green, Cl; red, O; yellow tetrahedron, AsO_4.

The title phases were grown in molten-salt media,[6] and their single-crystal structures[7] were determined by X-ray diffraction (XRD) methods. Further experimental details of XRD may be found in a recent publication.[8] Crystallographic data and atomic parameters are listed in Tables S1 and S2, respectively, in the Supporting Information (SI).

All three families of compounds share the same structural features and connectivity. As indicated by the structural composition of $\mathbf{V_5}$, (salt)·$Cs_{2.64}(V_5O_9)(AsO_4)_2$, the porous framework (Figure 1A) is made of periodic arrays of pentameric $[V_5O_{17}]$ units (Figure 1B) that are interconnected via shared vertex oxygen atoms of the AsO_4^{3-} tetrahedral units (Figure 1C). The metal halide salts reside in interconnected channels that run along three directions: [111] (Figure 1A), [110] (Figure S1 in the SI), and [001] (Figure S2 in the SI). Large cavities, formed at the channel intersections, lead to salt disorder determined by cation and anion vacancies consistently observed in multiple structure solutions. No trend can be found between the cell volume and ion

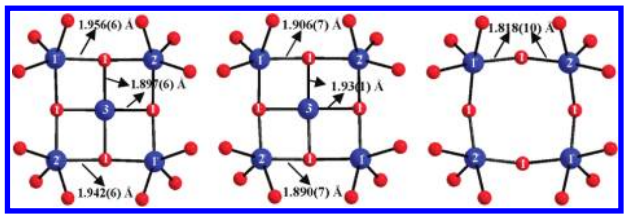

Figure 2. Projected view of the POV units in $\mathbf{V_5}$ (left), $\mathbf{V_{4/5}}$ (middle), and $\mathbf{V_4}$ (right). An increase in the average oxidation state of the V cations within the cores leads to an observed decrease in the V−O^b and V−V distances (see Table S5 in the SI). The V(3)═O apical bonds are not shown for clarity.

stoichiometry (Table S3 in the SI). This is because the former, not only affected by the number of ions, is also influenced by the ordering and packing efficiency of the salt.

A fascinating salt lattice, with an idealized composition $Na@Cl_8@Cs_{12}$ (Figure 1D), was found in a cavity at the intersection of the interconnected channels. It adopts O_h point symmetry, with ions occupying 50%, 75%, and 100% of the respective crystallographic sites. $Na@Cl_8@Cs_{12}$ has Cs_4 square planes that act as a template, directing the orientation of six capping $[V_5O_{17}]$ POV units (see Figure S3 in the SI) via Cs−O bonds.

The $[V_5O_{17}]$ unit exhibits a bowl-like structure (Figure 1C), enabling the formation of a circular porous framework. The alternating V(1)O_5 and V(2)O_5 square-pyramidal units share two corner oxygen atoms with one another and one edge with V(3)O_5, leading to four μ_3-oxo bridges per $[V_5O_{17}]$ unit (Figure 1B). The VO_5 units have short vanadyl V═O bonds that are comparable to the reported values. The charge of the $[V_5O_{17}]^{n+}$ unit varies slightly from crystal to crystal depending upon the concentration of cation vacancies (n) found. This correlation is reflected in the general formula (salt)·$Cs_{(6-n)}(V_5O_9)^{n+}(AsO_4)_2$. Bond valence sum calculations (Table S4 in the SI) suggest that the charge of the $V^{4+/5+}$ ions is delocalized.

$\mathbf{V_{4/5}}$ and $\mathbf{V_4}$ further reveal the complexity and versatility of this chemical system. These two new phases were isolated serendipitously in attempts to investigate the phase compatibility of the (salt)·$Cs_{(6-n)}(V_5O_9)^{n+}(AsO_4)_2$ series [see Figure S4 in the SI for powder XRD (PXRD) patterns and synthetic details]. Structural analysis of these in essence oxidative derivatives of $\mathbf{V_5}$ showed defects (vacancies) in the V(3) site, leading to modified POV structures, i.e., $[V_{5-x}O_{17-x}]$ ($x = 0.4$ and 1, respectively). As revealed in Figure 2, the respective POV units can formally be expressed by the sequence of oxidation $[V_5^{4.27+}O_{17}]^{12.64-}$ ($\mathbf{V_5}$) → $[V_{4.6}^{4.39+}O_{16.6}]^{13.01-}$ ($\mathbf{V_{4/5}}$) → $[V_4^{5+}O_{16}]^{12-}$ ($\mathbf{V_4}$). The $[V_{4.6}O_{16.6}]$ unit represents a statistical mixing of 60% $[V_5O_{17}]$ and 40% $[V_4O_{16}]$. Nonetheless, a decrease in the V−O^b and V−V distances and V−O^b−V angle within the POV core is evident, indicating an increase in strain within the core (see Table S5 in the SI) and, consequently, creating more vacancies in the V(3) site upon further oxidation.

The title compounds exhibit facile ion transport through their sizable channels. To demonstrate that, $\mathbf{V_5}$ ($x = 3.5$ set in stoichiometric yield synthesis) was soaked in water to yield a salt-free phase $Cs_{2.5}(V_5O_9)(AsO_4)_2·7.0H_2O$ (see the PXRD and EDX plots and TGA in Figures S5 and S6, respectively, in the SI). Subsequent oxidative removal of charge-balancing Cs^+ cations was carried out by soaking the resulting solid in H_2O_2/H_2O or I_2/CH_3CN solutions in

(6) Crystals (dark greenish blue in color) of $\mathbf{V_5}$ were grown by employing a eutectic CsCl/NaCl flux in a fused silica ampule under vacuum. Aldrich $CsVO_3$, VO_2, Cs_3VO_4, and As_2O_5 were mixed in a 1:3.5:0.5:1 mole ratio (ca. 0.5 g), and then the resulting mixture was added to a salt flux equal to 2 times the mass of the oxide reactants. The reaction was heated to 600 °C at 1 °C/min, isothermed for 3 days, and then slowly cooled at −6 °C/h to room temperature. Crystals of $\mathbf{V_{4/5}}$ (blue-green) and $\mathbf{V_4}$ (red) can be grown under the same conditions by employing ca. 0.5 g of $CsVO_3$, V_2O_5, and As_2O_5 with a respective mole ratio according to the formula (salt)·$Cs_{(6-n)}(V_5O_9)(AsO_4)_2$, $n = 4.5$ and 6.

(7) Crystal data (cubic, space group $Fd\bar{3}m$ (No. 227), $Z = 48$): $Cs_{3.50}Na_{1.47}(V_5O_9)(AsO_4)_2Cl_{2.33}$ ($\mathbf{V_5}$), $M_r = 1257.97$, $a = 33.119(4)$ Å, $V = 36{,}329(7)$ Å^3, $\rho_{calcd} = 2.760$ g/cm^3, final $R = 0.0707$, $R_w = 0.1976$, GOF = 1.044 (all data), 108 parameters; $Cs_{3.88}Na_{0.12}(V_{4.6}O_{8.6})(AsO_4)_2Cl_{0.99}$ ($\mathbf{V_{4/5}}$), $M_r = 1195.9$, $a = 32.957(4)$ Å, $V = 35797(7)$ Å^3, $\rho_{calcd} = 2.663$ g/cm^3, final $R = 0.1055$, $R_w = 0.2601$, GOF = 1.013 (all data), 108 parameters; $Cs_{3.64}Na_{1.40}(V_4O_8)(AsO_4)_2Cl_{3.04}$ ($\mathbf{V_4}$), $M_r = 1234.05$, $a = 32.742(4)$ Å, $V = 35101(7)$ Å^3, $\rho_{calcd} = 2.802$ g/cm^3, final $R = 0.1030$, $R_w = 0.2483$, GOF = 1.737 (all data), 108 parameters.

(8) West, J. P.; Hwu, S.-J.; Queen, W. L. *Inorg. Chem.* **2009**, *48*, 8439–8444.

the following reaction:

$$Cs_{2.5}(V_5O_9)(AsO_4)_2 + 1.25X_2 \rightarrow (V_5O_9)(AsO_4)_2 + 2.5CsX, \quad \text{where X = OH, I}$$

(see the PXRD patterns in Figure S7 in the SI). EDX shows that a small quantity of Cs^+ remains in the solid, signaling an incomplete oxidative deintercalation. It is thought that a certain amount of charge-balancing Cs^+ cations remains because further oxidation of the $[V_5O_{17}]^{n+}$ core would induce strain that, in the high-temperature reactions of $\mathbf{V_{4/5}}$ and $\mathbf{V_4}$, results in observed vacancies in the V(3) site.

Further attempts to synthesize a neutral-framework solid were made by substituting the apical vanadium, V(3), with lower-oxidation-state cations. The target composition was derived from the chemical formula of $\mathbf{V_4}$, i.e., (salt)·$(V_4MO_8)(AsO_4)_2$, where M = Cu^{2+} and, for comparison, Ni^{2+}. The PXRD patterns (Figure S8 in the SI) and EDX results suggest a partial inclusion of Cu^{2+}, as illustrated in the following chemical equation:

$$2V_2O_5 + CuO + As_2O_5 + (3-3x)CsCl \xrightarrow{\text{xs salt}} (\text{salt})\cdot Cs_{2-2x}(V_4Cu_xO_8)(AsO_4)_2 + (1-x)CsCuCl_3$$

Ni^{2+} inclusion was thought to be energetically less favorable because the adopted coordination site is significantly deviated from square-planar geometry, as evidenced by the $\sum(\angle O(1)^b-V(3)-O(1)^b)$ of ~337° in $\mathbf{V_5}$ and $\mathbf{V_{4/5}}$ (Table S5 in the SI). However, like the Cu^{2+} reaction, it yielded a green polycrystalline powder, as opposed to the red observed for $\mathbf{V_4}$, suggesting the incorporation of Ni^{2+}.

The as-prepared (salt-containing) $\mathbf{V_5}$ has a measured SA of 111(2) m^2/g, which is on the same order of magnitude as the theoretical value, 183 m^2/g (see the summary of SAs and theoretical approximation in Table S6 in the SI), estimated from the volume of voids given by the structural solution using the PLATON SQUEEZE function.[9] Relatively high SAs, ~90−110 m^2/g, were also measured in other as-prepared polycrystalline samples, confirming the existence of large void space (Table S6 in the SI).

Upon salt removal and redox chemistry in aqueous and organic media, new solids with expanded void space and, in turn, SAs (by ~35−70%) were readily acquired from $\mathbf{V_5}$ at room temperature. Dehydration of the new solid $Cs_{2.5}(V_5O_9)(AsO_4)_2\cdot 7.0H_2O$ acquired from soaking (salt)·$Cs_{2.5}(V_5O_9)(AsO_4)_2$, $\mathbf{V_5}$, in water leads to a 35% increase in the SA, from 111(2) to 150(2) m^2/g. This significant increase indicates the strong rigidity of the framework because it maintains a large cell volume upon removal of the salt. The oxidative deintercalation of Cs^+ from the soaked $\mathbf{V_5}$ samples in I_2/CH_3CN and H_2O_2/H_2O showed 25% and 61% increases in the SAs, 188(3) and 242(4) m^2/g, respectively.

Relatively high SAs were similarly observed for the soaked (salt)·$Cs_{6-n}(V_5O_9)(AsO_4)_2$ ($n = 4, 4.5$) samples, e.g., 120.3(8) and 129(1) m^2/g, respectively. These lower values than the observed SA for the soaked $\mathbf{V_5}$, 150(2) m^2/g, can be attributed to the presence of low-SA "impurity" phases (see the footnote in Figure S4 in the SI) and the more condensed $\mathbf{V_4}$ framework (Table S3 in the SI). It is thought that, upon oxidation, the POV units in $\mathbf{V_4}$ become more curved, causing a decrease in the cage volume and thus a slightly lower measured SA.

An increase in the SA was observed when comparing the soaked $\mathbf{V_4}$, 66(2) m^2/g and Cu-insertion phase (salt)·$Cs_{2-2x}(V_4Cu_xO_8)(AsO_4)_2$, 154(1) m^2/g, as shown in Table S6 in the SI(also see the cell parameters in Table S3 and PXRD patterns in Figures S8 and S9 in the SI). This further supports Cu^{2+} incorporation into the $[V_4O_{16}]$ unit and a decrease in the number of charge-balancing Cs^+ cations ($2x$). Thus, further pursuit of different methods to create a neutral framework is thought to be worthwhile because complete elimination of the charge-balancing Cs^+ cations could lead to the highest achievable SA of the material. It should also be noted that the SA of the unsoaked Ni^{2+}-containing phase showed an SA, 89(2) m^2/g, comparable to that of the Cu analogue, 90(2) m^2/g.

As final remarks, salt-inclusion synthesis has provided a means to prepare thermally stable mesoporous solids that, despite a high-temperature synthesis, have a relatively high Brunauer−Emmett−Teller SA. Multiple crystals grown under different reaction conditions were examined, confirming that "salt disorder" and "cation/anion vacancies" are intrinsic to these mesoporous structures. The title compounds are the first SISs showing electropositive cation to oxide bonds at the interface, Cs−O in this case. In all previous examples, where the framework is made of mid- and late-transition-metal (M) oxides, interactions were elucidated by M−Cl bonds, such as Mn−Cl and Cu−Cl.[4d−i] The absence of V−Cl bonds could be attributed to the lack of d electrons. Despite the observed SAs, preliminary experiments performed at low temperature, 87 K, and high pressures, up to 47 bar, have shown minimal H_2 adsorption. Nonetheless, these exciting discoveries offer insight into the synthesis of, for instance, open-framework vanadates for energy-related research such as water-splitting catalysis. We anticipate the synthesis of more novel porous solids given the demonstrated utility of salt-inclusion chemistry, incorporation of high-nuclearity POVs, and structural rigidity of the all-inorganic system.

Acknowledgment. This work has been supported by the National Science Foundation (NSF; Grants DMR-0322905 and -0706426). Support from the NSF for the purchase of a Micromeritics ASAP 2020 (partially by Grant DMR-0322905) and an X-ray diffractometer (Grants ESR-9108772 and CHE-9207230 and -9808165) is also gratefully acknowledged. We acknowledge support of the National Institute of Standards and Technology, U.S. Department of Commerce, in providing research facilities used in this work and Dr. Craig Brown for carrying out H_2 adsorption studies. S.R. thanks the Clemson Summer Undergraduate Research Program for financial support (Grant DMR-0755005).

Supporting Information Available: X-ray crystallographic file (in CIF format), procedures of stoichiometric synthesis, and figures of PXRD and TGA plots. This material is available free of charge via the Internet at http://pubs.acs.org.

(9) The void space was calculated to be 2609 $Å^3$, approximately 7.2% of the overall unit cell volume. There are eight equivalent cavities with an approximate volume of 326 $Å^3$ each. (a) Spek, A. L. *Acta Crystallogr.* **1990**, *A46*, C-34. (b) Spek, A. L. *A Multipurpose Crystallographic Tool*; Utrecht University: Utrecht, The Netherlands, 2002.